NASA Technical Memorandum 100159

Airflow Calibration and Exhaust Pressure Temperature Survey of an F-404, S/N 215-209, Turbofan Engine

Maureen E. Burns and Thomas A. Kirchgessner
Lewis Research Center
Cleveland, Ohio

September 1987

NASA

AIRFLOW CALIBRATION AND EXHAUST PRESSURE/TEMPERATURE SURVEY OF AN F-404, S/N 215-209, TURBOFAN ENGINE

Maureen E. Burns and Thomas A. Kirchgessner
National Aeronautics and Space Administration
Lewis Research Center
Cleveland, Ohio 44135

SUMMARY

A General Electric F-404 turbofan engine was calibrated for thrust and airflow at the NASA Lewis Propulsion System Laboratory in support of future flight tests of the X-29 aircraft. Tests were conducted with and without augmentation, over a range of flight conditions, including the two design points of the airplane. Data obtained during the altitude tests will be used to correct two independent gross thrust calculation routines which will be installed and operated on the airplane to determine in-flight gross thrust.

Corrected airflow data as a function of corrected fan speed collapsed onto a single curve. Similarly, trends were observed and defined for both augmented and dry thrust. Overall agreement between measured data and F-404 Engine Spec Deck data was within 2 percent for airflow and 6 percent for thrust. The results of an uncertainty analysis for thrust and airflow is presented.

In addition to the thrust calibration, the exhaust gas boundary layer pressure and temperatures were surveyed at selected condition and engine power levels to obtain data for another NASA F-404 program. Test data for these surveys are presented.

INTRODUCTION

The X-29 Forward Swept Wing aircraft program is a joint effort involving NASA, USAF, DARPA, Grumman, and Computing Devices Corp., a division of Control Data Canada, Ltd., (ComDev). In support of the future performance flight tests at Dryden Flight Research Facility, a General Electric F-404 turbofan engine was calibrated for thrust and airflow at the NASA Lewis Propulsion System Laboratory (PSL). Determination of in-flight thrust is one of the highest priorities of the X-29 program. At steady state flight condition, engine thrust equals aircraft drag; thus, in order to effectively evaluate aircraft performance, it is imperative that engine thrust and airflow be accurately known over the entire flight test envelope.

During flight, engine gross thrust will be calculated with the standard General Electric F-404 In-Flight Thrust Deck (IFTD). ComDev has developed another in-flight gross thrust calculation method which will be modified for use on the X-29. This method, called the Thrust Computing System (TCS), and the IFTD will be calibrated using test cell data to more closely represent the flight engine. Similarly, the General Electric F-404 Engine Spec Deck, which calculates additional operational and performance characteristics, will be

corrected for this engine. The airflow, thrust, and pressure data presented here will afford the means for correcting these computer programs.

All test data were obtained at steady state conditions, with and without thrust augmentation over a range of flight conditions. Test conditions were chosen to represent those scheduled for flight test. Flight Mach number ranged from 0.4 to 1.8 and altitude ranged from 3 050 to 13 720 m (10 000 to 45 000 ft). Nonstandard day as well as standard day inlet temperature effects were investigated.

Test results are presented in terms of corrected airflow and gross thrust as a function of corrected fan speed for nonaugmented power. Corrected gross thrust for augmented power is presented as a function of augmentor fuel-air ratio. Comparisons of the measured and predicted gross thrust data are presented, along with the results of an uncertainty analysis for measured corrected airflow, gross thrust, and pressure data required for the TCS algorithm.

The tests at Lewis provided an opportunity to obtain F-404 exhaust nozzle jet boundary pressure and temperature data required for another NASA program. During the airflow and thrust calibration tests, surveys of pressure and temperature at several power settings (up to full augmentation) were taken at the exhaust nozzle exit. The data obtained in these surveys are presented as a function of exhaust nozzle exit radius ratio.

APPARATUS

Engine

The F-404-GE-400 engine (S/N 215-209) used in this calibration test program is a Qualification Test flight test engine. Although it is a development engine, it is comparable to the production F-404 engine in all respects concerning performance and operation.

The F-404 is a twin-spool, low-bypass turbofan with an afterburner. The engine has a three stage fan and a seven stage compressor, each driven by a single stage turbine. The sea level static augmented thrust rating of the engine is 71 kN (16 000 lbf).

Engine control is provided by an integrated hydro-electromechanical system. The system provides power modulation from cutoff through maximum afterburning and schedules compressor speed, variable geometry, exhaust nozzle area, and afterburner fuel flow. The system also provides protection against exceeding the critical operating limits.

An altitude pressure signal, normally supplied from the aircraft, is needed for maximum engine temperature and fan speed trim. For the Lewis test, this signal was supplied from a power supply mounted in the control room and regulated by a manual potentiometer. For documentation purposes, this voltage signal was patched into the data recording system.

Facility

The tests were conducted in altitude test chamber 4, one of the two operational cells at the Propulsion System Laboratory (PSL). Each test chamber is 11.9-m (39-ft) long and 7.3 m (24 ft) in diameter. Conditioned air is supplied from a central air facility for the simulation of engine inlet conditions. The central air system also supplies the low pressure (vacuum) required to simulate desired altitude. A number of Lewis Research Center test facilities are serviced by the large electric motor-driven centrifugal compressors and exhausters which make up the central air system.

The inlet air temperature and pressure were regulated from the central air facility control room. However, the test pressures (i.e., both engine inlet and simulated altitude) were independently regulated by throttling valves controlled from the PSL control room.

The engine installation in the altitude test chamber is shown in figure 1. The engine was supported by an overhead mount coupled to the thrust bed. The bed was suspended from the test chamber by four flexure rods. The bed was free to move except as restrained by a dual load cell system which had the provision for preload.

A bulkhead at the inlet to the test chamber separated the chamber from an inlet plenum (5.5-m (18-ft) diam). Air at the desired pressure and temperature flowed from the plenum to the engine through a bellmouth and inlet duct. A labyrinth seal was used to isolate the inlet duct from the bellmouth and inlet bulkhead in order to provide a metric break for the thrust measuring system. To minimize the loading on the engine inlet flange, the inlet duct was coupled to the flange with a flexible rubber membrane. To minimize exhaust gas recirculation in the test chamber, a collector extending through the chamber rear bulkhead was used to capture the exhaust gases for passage to the facility exhaust system.

Compressor Bleed System

The calibration tests were performed with compressor discharge outflow bleed to simulate the bleed extraction of the X-29 cockpit and environmental control system. The desired constant bleed of approximately 0.20 kg/sec (0.45 lbm/sec) was maintained at military power and above for the majority of the test conditions. Previously acquired data in another facility indicated that bleed extraction of even this low magnitude might measurably affect the engine pressures upon which the TCS algorithm is dependent.

The bleed system components, chosen to withstand the engine compressor seventh-stage temperature and pressure conditions, consisted of a shutoff valve, control valve, and an instrumented flow-measuring orifice run (1.27-cm-(0.5-in.-) diameter orifice). The system was connected to the engine with a 5.1-cm-(2-in.-) diameter metal flex hose to provide for thermal growth and vibration isolation. Bleed airflow was directed radially from the engine so as not to interfere with axial thrust measurements.

Exhaust Nozzle Traversing Probe

The apparatus used to obtain the exhaust nozzle pressure and temperature survey data is shown in figure 2. The water-cooled body holding the three total pressure sensors and the two thermocouples was mounted vertically on a motor-driven actuation system which provided for both lateral and vertical movement. The pressure and temperature probes were located approximately 2.5 cm (1 in.) downstream from the exhaust nozzle exit plane (for the maximum nozzle area condition) during hot operation.

The configuration of the probes is shown in figure 3. The three total pressure sense tubes were platinum - 13 percent rhodium alloy, 0.32-cm-(1/8-in.-) outside diameter, and 25.0-mm-(0.010-in.-) wall thickness. The two nonshielded, wedge-type thermocouples consisted of 51.0-mm-(0.02-in.-) diameter iridium-iridium 40 percent rhodium thermocouple wire with the measuring junction bead extending 63.0 mm (0.25 in.) beyond the aluminum oxide insulation. The aluminum oxide insulation was contained within 0.32-cm-(1/8-in.-) outside diameter, 25.0-mm (0.010-in.) wall platinum 13 percent rhodium sheathing.

Instrumentation

Since the physical integrity of the flight engine was to be maintained, a minimal amount of engine instrumentation was used in this program. Measurements were made as necessary to set test conditions, monitor engine health, measure airflow and thrust, and obtain the augmentor duct and altitude pressure data required for the TCS algorithm.

The location of the inlet and engine pressure and temperature measurements are shown in figures 4(a) to (m). The measurements shown at station 5.6, 6.0, and 7.0 were required for the TCS algorithm. Refer to appendix A for a list of symbol definitions.

The instrumentation not shown in figure 4 includes the engine and facility-mounted fuel flow meters, fan and compressor speed sensors, engine variable geometry position indicators, vibration sensors, and load cells. In addition, figure 4 does not include the pressure and temperature instrumentation required to monitor general engine health, measure compressor bleed flow, or exhaust gas conditions. (Refer to the previous subsection for traversing probe instrumentation details.)

All data, including measured and calculated parameters were monitored and recorded in engineering units with the facility steady-state data system. The system, capable of updating every second, provided real-time CRT display of data as well as printed output of time-averaged data points. "Updating" refers to sampling instrumentation, converting to engineering units, calculating parameters, and displaying the information. A single steady-state data point consisted of the average of 10 updates of the system; each data point was stored on tape for permanent legal record. For post-run analysis, the data were loaded into an IBM 370 mainframe, where information could be validated and reprocessed for transmittal on magnetic tape.

TEST PROCEDURES

Engine Conditions

Engine inlet pressure and temperature and test chamber pressure were determined by the Mach number and altitude of interest in the X-29 flight program. Inlet pressure recovery factors as specified by NASA Dryden, were used to account for the specific X-29 inlet configuration. The inlet total pressure and temperature settings were based on the average of four measurements at the locations shown in figure 4(g) (station 2.0, engine inlet). The altitude was based on the average of the four static pressure measurements taken at the exterior of the exhaust nozzle (station 9.0). A listing of the simulated altitude test conditions is presented in table I.

Calibration Test

The engine calibration data at each condition were taken following a 10-min heat soak at Intermediate Rated Power (IRP or IM). All points below IM were approached from the high side by decreasing engine speed, and set according to the desired high compressor speed. The general procedure followed was to allow the engine to stabilize for 4 min prior to taking afterburner data.

Exhaust Survey Test

Two horizontal exhaust surveys were made at each condition and engine power setting. One traverse was made across the horizontal radius of the exhaust gas jet as shown in figure 5(a). The other traverse was made across the jet first quadrant as shown in figure 5(b). In this case, the rake was positioned vertically so that the center probe PT9C would intersect the exhaust jet boundary at 45° with respect to the horizontal diameter. In both cases, the survey was made across the exhaust jet boundary and inward to the vertical exhaust centerline.

The exhaust survey data recordings were made as soon as the survey rake pressure and temperature readings reached equilibrium following probe movement to the new survey point. It was possible to traverse to the new survey point and stabilize and record data at approximately 1 minute intervals.

Calculation Programs

For the flight tests of the X-29, two independent methods of in-flight gross thrust calculation will be used - the General Electric In-Flight Thrust Deck (IFTD) (ref. 1) and the ComDev Thrust Computing System (TCS).

The G.E. IFTD is a generic program representing a baseline F-404 engine. The performance of actual engines would be slightly different than that computed by the program. Using various engine and flight condition parameters, it calculated gross thrust with two gas generator techniques. All inputs, with the exception of flight Mach number and altitude, were provided by flight instrumentation mounted on the engine and recorded during the altitude tests. Prior to running, the IFTD was modified with the X-29 inlet pressure recovery

data obtained from previous wind tunnel model testing. The ComDev TCS, also referred to as the Simplified Gross Thrust Method (SGTM), provides an independent method of in-flight calculation on the X-29. The SGTM has previously been developed for the J-85 afterburning turbojet and the F-100 and TF-30 afterburning turbofans, each time with successful results. It requires fewer and simpler engine measurements than for a gas generator technique and is much less complex than the two algorithms of the IFTD. The program calculates gross thrust based on a one-dimensional simplified analysis of the flow. Measured pressures in the tailpipe (stations 5.6, 6.0, and 7.0) and measured ambient pressure are inputs to the algorithm; two-dimensional and nonideal effects, such as friction, mass transfer, and area change are accounted for in empirically determined calibration constants, which vary with engine operation and flight conditions.

Requirements during the initial planning stages of this calibration included on-line operation of the two thrust decks as integral parts of the facility data system and reduction program. However, given the complexity of the G.E. deck, the data system cycle update time (1 cycle/sec) would have been compromised if the deck were run on-line. The decision was made to use only the simpler ComDev TCS algorithm on-line and do post-run correction to the G.E. deck with the acquired test data.

RESULTS AND DISCUSSION

The two phases of the test, the engine calibration and the exhaust survey, were conducted with and without afterburning for a variety of engine and flight conditions. For the airflow-thrust calibration, emphasis was placed on the two design conditions of the X-29; that is, Mach 0.9 and 1.2 at 9140-m (30 000-ft) altitude. For the exhaust survey, the emphasis was placed on obtaining data in the boundary layer region of the plume at flight conditions in the upper left hand corner and central area of the flight envelope.

Airflow and thrust data were corrected to inlet conditions then normalized with appropriate design constants. For corrected airflow, a constant of 68.0 kg/sec (150 lbm/sec) was used, and for corrected gross thrust, a constant of 71 kN (16 000 lbf) was chosen. Corrected augmented thrust is normalized to corrected intermediate thrust at the same flight condition. For the exhaust survey data, radial position is normalized to the calculated radius of the nozzle exit at that condition.

Standard Day

Corrected airflow as a function of corrected fan speed is presented in figure 6. The various Mach number-altitude conditions represent inlet Reynolds number indices from 0.96 to 0.34. A range of corrected fan speeds from part power, approximately 7000 rpm, to intermediate was investigated, with all data collapsing onto a single curve. Little scatter was observed, and no apparent shift is seen from one condition to another.

The corrected nonaugmented thrust data (fig. 7) differs in that each condition represents a distinct curve. Again, a range of corrected fan speeds

from 8500 rpm to intermediate was investigated. There are several things to note about the data presented here as follows:

(1) Flight idle thrust data were disregarded because at the low power level, thrust levels were low and accurate measurements were difficult to make.

(2) For the condition of 9140 m (30 000 ft) and Mach 1.2, the "N2 Lockup" was engaged. This feature, built into the engine control, would prevent rotor speeds from decreasing significantly with a decrease in power lever angle (PLA) below intermediate. Therefore, data taken at PLA below 87° (intermediate) appears not to change as much as at other conditions.

(3) Although data were taken at more conditions than are presented on the plot, there were not enough points at each of the conditions to adequately describe the curve for presentation. It is sufficient to say that the data presented here are indicative of normal engine operating trends.

Corrected gross thrust increased with increasing Mach number for a given fan speed. For example, at 9140 m (30 000 ft) and corrected fan speed of 12 250 rpm, corrected thrust/nominal gross thrust is 0.475 for Mach 0.5, and 0.5 for Mach 0.9. At constant Mach number and fan speed, an increase in altitude produces a decrease in thrust. For example, at Mach 0.8 and fan speed of 13 000 rpm, the thrust ratio is 0.65 at an altitude of 3050 m (10 000 ft), and 0.60 at an altitude of 12 190 m (40 000 ft).

Augmented thrust data are presented in figure 8. Figure 8(a) shows all nine conditions at which augmented data were gathered, and figures 8(b) and (c) break the group of nine into two smaller groups so that the data are more clearly displayed. Afterburner (AB) data at each condition were taken at PLA of 94° (min. AB), 100, 110, 120, and 130° (max. AB). The exception is 3050-m (10 000-ft) altitude and Mach 0.8 where an increase in PLA past 120° resulted in load cell overrange.

The data, the ratio of corrected gross thrust to the corrected intermediate thrust at the same condition are plotted as a function of afterburner fuel-air ratio. (See appendix B for calculation of fuel-air ratio.) Note that this calculation is very sensitive. Accurate readings of the large capacity afterburner fuel flowmeters for low flow rates was at some times very difficult. Still, the data scatter was small enough so that distinct curves could be defined. As expected, all curves originate from the intermediate power point of thrust ratio equal to one and fuel-air ratio in the afterburner of zero. Except for the fact that thrust increases with power lever angle for each condition, no general trends are obvious. This could be due to such variables as flight Mach number, inlet temperature changes, nozzle area, and fuel flow variation, which could disturb the sensitive fuel-air calculation and thrust levels.

Nonstandard Day

The effect of a nonstandard inlet temperature variation was explored at two of the flight conditions, Mach 0.6 at 6100 m (20 000 ft), and Mach 0.9 at 9140 m (30 000 ft). Air entering the engine was varied ±10.77 K (20 °F) from the standard day temperature, and data were obtained over a range of power

lever angles from part power to maximum afterburning. Similar to the standard day data, the corrected airflow and gross thrust data are plotted as a function of corrected fan speed for nonaugmented power, and augmented thrust is plotted as a function of afterburner fuel-air ratio (figs. 9 to 11). Again, the airflow data collapsed onto a single curve, with little deviation evident. Corrected nonaugmented gross thrust data, compared to standard day data appears to be higher at the hot inlet condition, and lower at the cold condition. However, the reverse appears true for augmented power, where thrust is higher at the cold condition, and lower at the hot condition. This trend is especially evident at the high fuel-air ratios of maximum afterburning.

Exhaust Gas Survey

Representative exhaust gas survey data are shown in table II. The uncorrected total pressure and temperature data obtained at two flight conditions at intermediate or military engine power (87° PLA) and at maximum afterburning (130° PLA) are presented. Two survey rake traverses were made at each flight and PLA condition. The rake horizontal and vertical positions, with respect to the engine exhaust nozzle centerline, are presented under the XSRL and XSRV tabular headings. The XSRL dimension is the lateral distance from the exhaust nozzle vertical centerline to the rake center pressure probe (PT9C). The XSRV dimension is the vertical distance from the exhaust nozzle horizontal centerline to probe PT9C. The rake was mounted vertically, and the vertical distance of the other four probes from PT9C can be deduced from the dimensions shown in figure 5.

The data of table II are presented in a more comprehensible form in figures 12 to 15. The measured exhaust gas pressures and temperatures for each flight condition and each engine power setting are shown plotted as a function of radius ratio (i.e., the probe radial position with respect to the nozzle centerline divided by the calculated nozzle exit radius).

It is seen that in all cases the pressure data correlates quite well as a function of radius. This indicates pressure profile symmetry across the exhaust jet region covered in these tests.

The temperature data for both maximum afterburning test cases also correlates well as a function of radius. However, for both of the military power test cases, the temperature correlation is not as good. Also, note that the temperature profile oscillations in all the traverses across the exhaust jet first quadrant are seen to be outside the exhaust jet boundary.

As previously stated, the probe radial position for each test point has been normalized with respect to the calculated nozzle exit radius (R9). The R9 value for each case is listed on the appropriate figure. The values were taken from the Engine Spec Deck calculations (ref. 2). The sharp rise in pressure across the exhaust jet boundary is readily apparent in each pressure data plot presented in figures 12(a) through 15(a). It is seen, also, that the actual jet radius is approximately 5 to 10 percent larger than the calculated R9 values in all cases. This is not unusual, since the Engine Spec Deck is uncorrected, and does not exactly represent this particular engine.

In addition to the exhaust survey data presented here, several exhaust surveys were made at partial afterburning power settings. A complete presentation of all the data is given in reference 3. The temperature and pressure data in that reference have been corrected for radiant heat loss, Mach number effects, and shock wave effects. The data presented here have had no corrections applied.

Data Comparisons and Accuracies

A preliminary comparison of test cell data as a function of calculated computer output is presented in figures 16 to 18. The computer output is that of the uncorrected General Electric IFTD (ref. 1), one of the programs to be calibrated with test cell data. (Since this computer deck is uncorrected, these comparisons are used merely as general references and should not be used to draw specific conclusions about this particular engine's performance and operation.) In addition, since data quality can be determined from measurement accuracy, a measurement and error analysis is presented here also.

Data comparisons. - A corrected airflow comparison is shown in two different ways in figures 16 and 17. Figure 16 is a direct comparison of airflow versus fan speed curves for both test cell data and computer output. The measured data follows very closely with the predicted values, especially at part power points up to 11 000 rpm. A larger difference is seen at higher airflow rates and fan speeds where measured data exceed that of the predicted airflow values.

Figure 17 is a more quantitative description of the qualitative figure 16. Data are shown for some standard day conditions, as well as the nonstandard day inlet condition at Mach 0.9, 9140-m (30 000-ft) altitude. Airflow deviation, which is measured value minus calculated (predicted) value divided by calculated value and expressed as a percent, is plotted against percent corrected airflow. The measure of dispersion of this data is described by the mean and standard deviation (σ) which are, respectively, 0.878 and 1.47. This indicated that 1 or 68.3 percent of the data fell within a band of width ± 1.47 about the mean value. Data agreement is very good throughout the range of fan speeds with the exception of a part power point and a few higher flow points where deviations of up to 3 percent were seen. This is consistent with the information of figure 16. Note also there is not a significant difference for nonstandard day data compared to standard day data.

The gross thrust comparison data are presented in figure 18. Data are shown for both dry and augmented thrust with solid points indicating augmented data. Thrust deviation, measured data minus calculated data divided by calculated data, is plotted against normalized thrust. Augmented gross thrust is referenced to nominal rather than intermediate thrust for figure 18. With a few exceptions, measured gross thrust is higher than predicted thrust values. The mean of the data is 3.14 and standard deviation is 2.07 indicating the agreement is not as good as that of airflow data. During testing, fuel properties such as lower heating value changed slightly from run to run. This is not reflected in the computer algorithm; thus, the higher variances are not surprising. In addition, predicted output for all power levels were not readily available and were interpolated from existing data. Still, agreement is

good, especially for augmented conditions where a large part of the data deviated from the predicted values by less than 2 percent.

Measured data uncertainty. - The results of an uncertainty and error analysis are presented in table III for corrected airflow and gross thrust. Propogation of error in the test cell data reduction program was determined by using instrument inaccuracies (see appendix B) and the weighted root-sum-square combination of these inaccuracies (ref. 4). Most of the uncorrected airflow uncertainty is less than 1 percent of the measurement. Corrected airflow uncertainty increases because of the additional uncertainty of the inlet measurements, but still remains lower than 1.5 with the exception of the high altitude (12 190 m (40 000 ft)) data. Gross thrust inaccuracies are shown for both intermediate and maximum attained power. Recall, with the exception of one condition, this maximum is 130° PLA (max. AB). For the condition of Mach 0.8 at 3050 m (10 000 ft), the maximum was 120° PLA. Uncertainties for gross thrust reached a maximum of 0.73 percent of measurement at the high altitude (low gross thrust) condition of 12 190 m (40 000 ft). Note also that uncertainties for thrust and airflow increased with decreasing Reynolds number index.

SUMMARY OF RESULTS

In summary of the calibration tests and exhaust survey, the principal results are as follows:

(1) For standard day conditions, all corrected airflow data collapsed onto a single curve as a function of corrected fan speed with little scatter or deviation.

(2) For standard day, corrected nonaugmented gross thrust increased with increasing fan speed and increasing flight Mach number, and it decreased with increasing altitude. However, no such pronounced trends were evident for augmented thrust.

(3) For nonstandard day inlet temperatures, corrected airflow and nonaugmented gross thrust correlated as expected with fan speed. Nonaugmented thrust appears higher for a hot day and lower for a cold day. However, compared to standard day conditions, augmented thrust appears higher for a cold day and lower for a hot day, especially at the higher augmentor fuel-air ratios of maximum afterburning.

(4) The exhaust survey data shows very good correlation between gas pressure and nozzle exit radius, as well as between gas temperature and exit radius. The boundary layer is clearly evident in this data.

(5) Comparisons of test cell data with uncorrected predicted values show very good agreement, especially for airflow. Airflow deviation was generally less than ±2 percent of predicted values, and thrust deviation was less than 6 percent. Augmented thrust was significantly better than nonaugmented data with deviations less than 2 percent.

APPENDIX A - SYMBOLS

A	area, cm^2
AB	afterburning
F_{area}	pressure-area forces of engine inlet, exit, duct flanges, etc., N
F_{defl}	spring forces of dual load cell system, N
F_{frict}	unknown forces due to assembly, cooling air, pressure differentials, etc., N
Fg	gross thrust, N
F_{ml}	main load cell reading, N
F_{mom}	force due to momentum of inlet airflow, N
F_{pl}	preload load cell reading, N
f/a	fuel-air ratio
g_c	units constant, kg-m/(N-sec^2)
IM	intermediate rated power (IRP)
Mo	flight Mach number
NFR	fan speed, rpm
P	pressure kn/m^2
PLA	power lever angle
PT9A	indicated pressure, traversing probe position A, kN/m^2
PT9C	indicated pressure, traversing probe position C, kN/m^2
PT9E	indicated pressure, traversing probe position E, kN/m^2
R	universal gas constant, J/kg-K
RNI	Reynolds number index $\delta/(\mu/\mu_{std})$
R9	calculated variable nozzle exit radius, cm
T	temperature, K
TT9B	indicated temperature, traversing probe position B, K
TT9D	indicated temperature, traversing probe position D, K
w	mass flow rate, kg/sec

γ	ratio of specific heat
δ	ratio of total pressure to sea level static pressure
θ	ratio of total temperature to sea level static temperature
μ	absolute viscosity, kg/m-sec
ρ	density, kg/m^3
σ	standard deviation

Subscripts

a	air
amb	ambient
aug	augmentor, or afterburner
calc	calculated from a computer deck
corr	corrected
e	engine
f	fuel
int	intermediate throttle setting
meas	measured value
nom	nominal value
s	static
std	standard sea level conditions
t	total
0	station 0, free stream
1	station 1, airflow measuring
2	station 2, engine inlet
5.6	station 5.6, turbine exit
6	station 6, augmentor duct (liner)
7	station 7, augmentor duct (liner)
9	station 9, nozzle exit

APPENDIX B - METHODS OF CALCULATION

Airflow

Total engine airflow was calculated by using a numerical method to integrate the flow at the engine inlet. Boundary layer pressure rakes were used to divide the inlet into eight annular sections, and the average Mach number and flow rate were calculated for each section (i) by using compressible flow equations (refs. 5 and 6). The trapezoidal rule was used to numerically integrate the flows across the inlet to obtain the total flow.

Average Mach number for a given annulus:

$$Mo,_i = \left\{ \frac{2}{\gamma - 1} \left[\left(\frac{P_{ti}}{P_{s1}} \right)^{\frac{\gamma-1}{\gamma}} - 1 \right] \right\}^{1/2}$$

Average annular mass flow rate:

$$w_i = (P_{ti}) Mo,_i \left[\frac{g_c \gamma}{R T_{t,2}} \left(\frac{P_{ti}}{P_{s1}} \right)^{-\frac{\gamma+1}{\gamma}} \right]^{1/2}$$

Total flow:

$$w_{a,1} = \Sigma (w_i)(A_i)$$

where

P_{ti} a boundary layer total pressure for a given annulus

P_{s1} station 1 static pressure

T_{t2} free stream total temperature

P_{t2} free stream total pressure

A area at airflow measuring rakes, station 1

Gross Thrust

The facility (measured) gross thrust was calculated as the sum of various forces as follows:

$$Fg = F_{mom} + F_{m1} - F_{p1} + F_{area} + F_{defl} + F_{frict}$$

where

F_{area} pressure-area terms of engine inlet, exit, and flanges of duct assembly (labyrinth seal, etc.)

F_{defl} spring force of dual load cell system

F_{frict} unknown forces due to factors such as facility cooling air impingement on engine, support structures and ducting, and pressure differential forces of assembly. These forces were determined in specific facility calibration exercises.

F_{ml} main load cell reading

F_{mom} inlet force due to momentum of airflow

F_{pl} preload load cell reading

Augmentor Fuel-Air Ratio

Fuel-air ratio in the afterburner was calculated as follows:

$$f/a = \frac{w_{f,aug} * \rho_{f,aug}}{w_{a,1} - \left(\frac{w_{f,e}}{stoic}\right)}$$

where

$w_{f,aug}$ augmentor fuel flow (main AB + pilot AB meters)

$\rho_{f,aug}$ density of fuel entering augmentor (function of temperature and specific gravity of fuel)

$w_{f,e}$ fuel flow to engine

$w_{a,1} - \left(\frac{w_{f,e}}{stoic}\right)$ unburned air entering afterburner

stoic stoichiometric fuel-air ratio, 0.06727

Measurement Uncertainties

The systematic error of airflow and gross thrust was found by using the root-sum-square combination of the instrumentation errors (ref. 4). The following values were obtained from a study of the facility instrumentation and data system (ref.7):

Free stream total temperature, T_{t2}, K(°R)	1.4 (2.52)
Station 1 static pressure, P_{s1}, kN/m^2(psia)	0.276 (0.014)
Free stream total pressure, P_{t1}, kN/m^2(psia)	0.276 (0.014)
Free stream total pressure, P_{t2}, kN/m^2(psia)	0.276 (0.014)
Station 9 static pressure, P_{s9}, kN/m^2(psia)	0.276 (0.014)
Main load cell reading, F_{m1}, kN (lbf)	0.133 (30)
Preload load cell reading, F_{p1}, kN (lbf)	0.133 (30)
Indicated pressure, PT9A, kN/m^2(psia)	0.138 (0.020)
Indicated pressure, PT9C, kN/m^2(psia)	0.138 (0.020)
Indicated pressure, PT9E, kN/m^2(psia)	0.138 (0.020)
Indicated temperature, TT9B, K(°R)	(a)
Indicated temperature, TT9D, K(°R)	(a)
Free stream total pressure, $P_{t5,6}$, kN/m^2(psia)	0.138 (0.020)
Station 6 static pressure, P_{s6}, kN/m^2(psia)	0.138 (0.020)
Station 7 static pressure, P_{s7}, kN/m^2(psia)	0.138 (0.020)

[a]These are Ir-Ir-Rh thermocouples. In the temperature range explored during the exhaust survey tests, the greatest error in measurement resulted from radiation effects. This error was corrected for by the test requestors in a separate report (ref. 3).

REFERENCES

1. F-404 In-Flight Thrust Deck. General Electric Deck No. 83112, version 8-08-83.

2. F-404 Engine Specification Deck. General Electric, Program No. 80031A(u), Aug. 26, 1981.

3. Walton, J.T.; and Burcham, F.W., Jr.: Exhaust-Gas Pressure and Temperature Survey of an F-404-GE-400 Turbofan Engine. NASA TM-88273, 1986.

4. Beckwith, T.G.; Buck, N.L.; and Marangoni, R.D.: Mechanical Measurements, Addison-Wesley Publishing Company, 1982.

5. Hesse, W.J.; and Mumford, N.V.S., Jr.: Jet Propulsion, Pitman Publishing Corp., 1964.

6. Hill, P.G.; and Peterson, C.R.: Mechanics and Thermodynamics of Propulsion, Addison-Wesley Publishing Company, 1970.

7. Abdelwahab, M.; and Biesiadny, T.J.; and Silver, D.: Measurement Uncertainty for the Uniform Engine Testing Program Conducted at NASA Lewis Research Center. NASA TM-88943, 1987.

TABLE I. - SIMULATED FLIGHT CONDITIONS

Simulated flight condition number	Mach number, Mo	Altitude		Inlet pressure, P_{t2}		Inlet temperature, T_{t2}		Ambient pressure, P_{amb}		Reynolds number index, RNI
		m	ft	kN/m^2	psia	K	°R	kN/m^2	psia	
1[a]	0.8	3 050	10 000	102.6	14.88	303	545	69.7	10.11	0.96
2	.6	6 100	20 000	57.4	8.32	266	479	46.5	6.75	.63
3[b]	.6	6 100	20 000	57.4	8.32	254	458	46.5	6.75	.67
4[c]	.6	6 100	20 000	57.4	8.32	278	501	46.5	6.75	.59
5	.9	7 310	24 000	64.1	9.29	280	504	39.3	5.70	.66
6[d]	.4	9 140	30 000	32.1	4.65	258	465	30.1	4.36	.37
7	.5	↓	↓	34.3	4.97	240	432	↓	↓	.42
8[e]	.9			49.1	7.12	266	479			.54
9[b]	.9			49.0	7.11	253	455			.57
10[c]	.9			49.1	7.12	279	502			.50
11[e]	1.2			72.2	10.47	295	531			.67
12	.8	12 190	40 000	27.6	4.00	244	440	18.8	2.72	.33
13	1.6	12 190	40 000	72.4	10.50	328	590	18.8	2.72	.61
14	1.8	13 720	45 000	69.4	10.06	357	643	14.8	2.14	.52

[a]Limited to 120° PLA.
[b]Cold day, -11 K (20 °R).
[c]Hot day, +11 K (20 °R).
[d]Exhaust survey data.
[e]X-29 design conditions.

TABLE II. - EXHAUST GAS SURVEY DATA

(a) Flight condition 5

Power lever angle, PLA, deg	Rake position		Pressure			Temperature	
	XSRL, cm	XSRV, cm	PT9A, kN/m^2	PT9C, kN/m^2	PT9E, kN/m^2	TT9B, K	TT9D, K
87	43.25	0.17	39.4	39.4	39.4	308	306
	30.37	.18	38.9	39.0	39.0	311	309
	28.20	.17	38.5	38.3	38.8	386	364
	26.81	↓	39.2	40.9	35.1	494	474
	26.20		47.5	83.2	36.5	655	483
	25.50		136.2	157.8	44.4	772	685
	24.13		177.6	177.6	170.8	807	783
	23.10	.18	184.1	180.1	179.4	856	822
	21.87	.16	184.1	182.5	179.9	909	869
	20.72	.18	187.3	193.9	184.3	944	894
	19.62	↓	198.6	198.3	197.9	971	916
	14.40		201.0	202.3	201.9	1033	1002
	9.90		198.2	199.6	201.4	1052	1041
	4.81	.17	197.4	197.3	199.8	1049	1042
	.88	.18	200.3	164.9	191.0	1042	1036
	.30	.17	200.5	161.2	191.8	1040	1034
	- .72	.18	200.1	171.8	195.6	1037	1033
	-1.11	.18	200.0	177.6	196.8	1036	1032
	27.67	14.40	39.9	39.9	39.2	361	385
	26.56	14.42	37.7	35.8	36.8	452	521
	25.32	14.41	36.6	35.0	40.4	537	518
	24.40	14.40	35.5	38.3	96.1	564	492
	22.83	14.42	37.1	39.7	169.4	485	784
	21.59	14.41	37.4	135.1	173.6	478	812
	20.20	14.40	38.2	169.2	175.2	540	861
	19.00	14.42	39.2	175.1	179.6	736	892
	17.81	14.41	44.9	177.2	189.5	738	921
	17.04	14.40	78.6	177.4	196.7	744	930
	16.21	14.42	151.8	179.4	200.1	756	934
	15.22	14.40	166.5	182.9	200.6	776	942
	14.37	14.41	172.5	189.1	199.8	794	950
	13.76	14.41	179.8	198.1	198.6	796	950
	11.15	14.40	178.6	198.2	198.4	832	963
	6.81	14.41	184.0	199.9	199.2	903	956
	3.35	14.40	193.0	200.6	199.9	929	975
	- .13	14.41	196.8	200.1	199.9	948	999
130	38.07	.17	39.9	39.9	40.0	411	368
	36.70	.17	37.6	38.6	35.1	684	607
	35.56	.18	55.2	84.0	39.2	1124	622
	34.34	.17	136.8	141.4	74.6	1414	1188
	32.52	.18	153.0	154.3	148.8	1830	1542
	30.63	.19	166.1	163.7	160.5	2034	1989
	29.21	.17	168.1	168.0	165.5	2020	2070
	27.37	.18	168.6	168.7	167.0	2022	2050
	19.93	.18	170.4	169.4	168.9	2022	2066
	14.50	.19	170.2	169.0	172.3	1986	2030
	7.62	.18	168.3	171.8	171.8	1997	2049

TABLE II. - Continued.

(a) Flight condition 5

Power lever angle, PLA, deg	Rake position		Pressure			Temperature	
	XSRL, cm	XSRV, cm	PT9A, kN/m^2	PT9C, kN/m^2	PT9E, kN/m^2	TT9B, K	TT9D, K
130	-3.37	0.17	171.4	190.2	173.0	1934	1992
	-1.92	.19	176.9	190.7	171.8	1928	1970
	-1.23	.18	178.4	191.1	171.7	1921	1962
	- .78	.18	178.9	173.0	171.2	1918	1960
	- .27	.18	179.3	128.5	169.6	1913	1956
	43.18	23.96	39.3	39.4	39.3	304	305
	37.05	↓	39.0	39.1	39.1	316	316
	35.80		38.3	37.0	35.2	430	543
	34.33		37.0	34.6	34.3	591	776
	33.15		36.0	34.0	39.1	755	806
	31.85		36.3	37.6	39.0	749	583
	30.64		36.3	38.4	79.9	748	578
	29.37		38.2	38.8	136.2	654	738
	28.09	↓	38.7	39.2	147.4	618	1290
	26.91	23.95	38.9	42.8	154.2	548	1433
	25.60	23.95	39.4	130.9	162.3	501	1614
	24.45	23.96	39.7	141.7	165.8	520	1766
	23.22	23.95	39.4	145.3	166.7	963	1869
	22.26	23.96	39.9	149.9	167.1	1163	1935
	20.76	23.96	52.3	155.9	166.5	1379	2035
	19.68	23.95	126.3	160.7	166.7	1545	2071
	14.27	23.96	157.4	166.8	167.7	2018	1992
	11.73	23.95	160.7	167.7	168.5	1957	1950
	5.44	23.96	163.4	165.6	167.0	1964	1998
	-3.12	23.96	164.8	168.4	168.0	1923	1988
	.21	23.95	167.5	167.4	167.7	1930	1989

TABLE II. - Continued.

(b) Flight condition 6

Power lever angle, PLA, deg	Rake position		Pressure			Temperature	
	XSRL, cm	XSRV, cm	PT9A$_2$, kN/m^2	PT9C$_2$, kN/m^2	PT9E$_2$, kN/m^2	TT9B, K	TT9D, K
87	31.34	0.02	30.1	30.0	30.3	287	287
	29.30	↓	30.1	29.8	30.2	287	287
	28.11		30.2	29.9	30.3	288	287
	26.82		29.8	29.3	30.1	389	353
	25.48		31.1	32.7	29.1	478	412
	24.26	↓	78.5	90.1	35.9	737	649
	22.98	.03	100.8	110.2	93.8	813	755
	21.94	.03	112.4	114.9	111.3	860	823
	20.70	.02	116.1	115.2	114.9	898	873
	19.63	↓	113.5	107.3	114.8	922	904
	18.55		110.5	107.9	109.9	938	921
	13.80		109.1	109.4	109.9	971	964
	9.60		108.9	108.6	109.9	977	980
	4.55	↓	112.0	111.5	112.6	978	985
	-.05	.03	113.9	100.7	111.2	975	979
	25.17	16.31	30.6	29.8	29.7	352	416
	22.75	16.30	28.2	28.1	30.2	461	412
	21.56	16.31	28.9	29.7	56.1	454	412
	20.53	16.29	30.0	30.1	98.8	410	541
	18.98	16.31	30.3	32.4	113.9	368	734
	17.87	16.31	30.0	69.7	116.9	383	766
	17.03	16.30	30.6	80.2	116.2	393	777
	16.30	16.32	30.3	93.3	114.8	417	792
	15.29	16.30	30.3	102.7	109.3	487	807
	14.55	16.32	30.2	108.8	109.9	602	822
130	36.46	.00	29.9	30.0	30.2	323	317
	35.52	.01	30.2	30.0	30.2	397	416
	34.44	.00	29.6	29.9	29.3	764	689
	33.32	.00	37.6	47.2	30.8	1088	956
	33.07	.01	48.9	63.4	33.5	1261	1087
	32.76	↓	57.0	76.1	39.1	1367	1163
	31.18		83.4	94.4	85.1	1640	1429
	29.92		100.1	96.2	97.6	1954	1812
	27.93		95.2	94.1	93.5	2003	2047
	26.34	↓	94.3	94.1	94.4	1998	2040
	19.75	.00	94.1	94.9	94.8	1898	1953
	13.24	.01	95.7	97.8	96.8	1909	1930
	6.56	.02	105.8	105.8	105.1	1852	1898
	-2.48	.01	104.1	101.8	104.1	1776	1825
	.07	.01	103.8	82.2	104.1	1762	1817
	43.92	23.11	30.4	30.2	30.3	296	296
	34.40	23.12	30.3	30.3	30.4	304	308
	32.96	23.18	30.1	29.9	29.6	319	432
	31.71	23.12	29.8	29.5	29.8	370	573
	30.39	23.11	29.9	29.0	30.2	497	639
	29.17	23.12	29.9	29.9	30.4	547	538
	27.98	23.11	30.2	30.2	49.9	413	550

TABLE II. - Concluded.

(b) Flight condition 6

Power lever angle, PLA, deg	Rake position		Pressure			Temperature	
	XSRL, cm	XSRV, cm	PT9A$_2$, kN/m^2	PT9C$_2$, kN/m^2	PT9E$_2$, kN/m^2	TT9B, K	TT9D, K
130	26.63	23.25	30.1	30.0	82.7	525	927
	25.44	23.12	30.0	30.0	91.7	527	871
	24.17	23.38	30.0	49.9	99.4	402	1265
	23.91	23.11	30.1	56.2	100.3	415	1352
	23.62	23.30	30.1	62.6	100.5	445	1427
	22.74	23.13	30.2	72.6	99.3	555	1539
	22.00	23.50	30.3	79.1	94.8	611	1679
	20.93	23.13	30.2	88.8	93.4	975	1848
	19.66	23.11	30.2	96.2	93.2	1278	1975
	18.55	23.13	30.8	101.2	93.0	1430	2030
	13.93	23.24	86.5	93.1	92.9	1927	2018
	9.20	23.31	101.7	93.5	93.8	1983	2002
	4.68	23.12	99.5	94.0	94.0	2011	2009
	.01	23.12	94.4	93.3	95.0	2024	2020

TABLE III. - MEASUREMENT UNCERTAINTIES

[As percent of measurement.]

Simulated flight condition	Gross thrust,		Airflow	Corrected airflow
	IM	max.		
3050 m (10 000 ft) Mo = 0.8	0.25	0.18	0.55	0.66
12 190 m (10 000 ft) Mo = 1.6	.47	.31	.84	.87
9140 m (30 000 ft) Mo = 1.2	.26	.20	.72	.77
7310 m (24 000 ft) Mo = 0.9	.34	.22	.77	.82
6100 m (20 000 ft) Mo = 0.6	.38	.26	.84	.89
9140 m (30 000 ft) Mo = 0.9	.42	.27	.97	1.02
9140 m (30 000 ft) Mo = 0.5	.62	.41	1.38	1.43
12 190 m (40 000 ft) Mo = 0.8	.73	.50	1.64	1.70
9140 m (30 000 ft) Mo = 0.9, hot day	.44	.29	.97	1.02
9140 m (30 000 ft) Mo = 0.9, cold day	.26	.26	.97	1.03

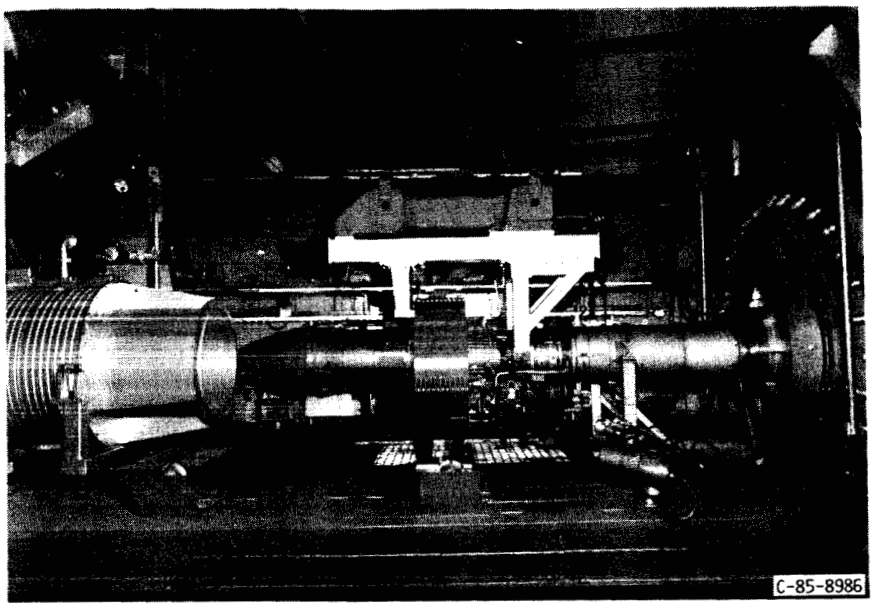

FIGURE 1. - ENGINE INSTALLATION IN THE TEST CHAMBER.

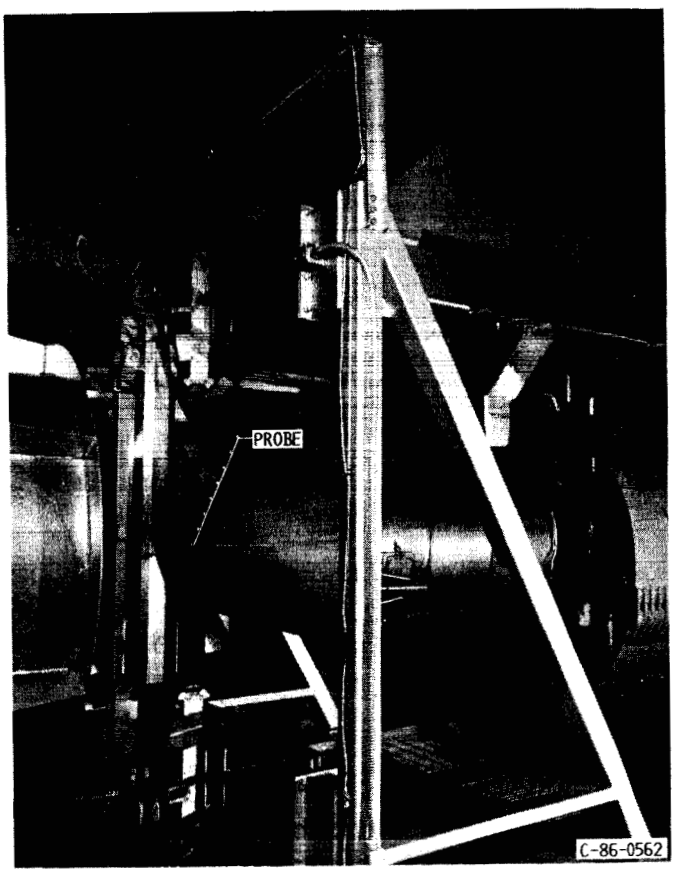

FIGURE 2. - EXHAUST NOZZLE TRAVERSING PROBE INSTALLATION.

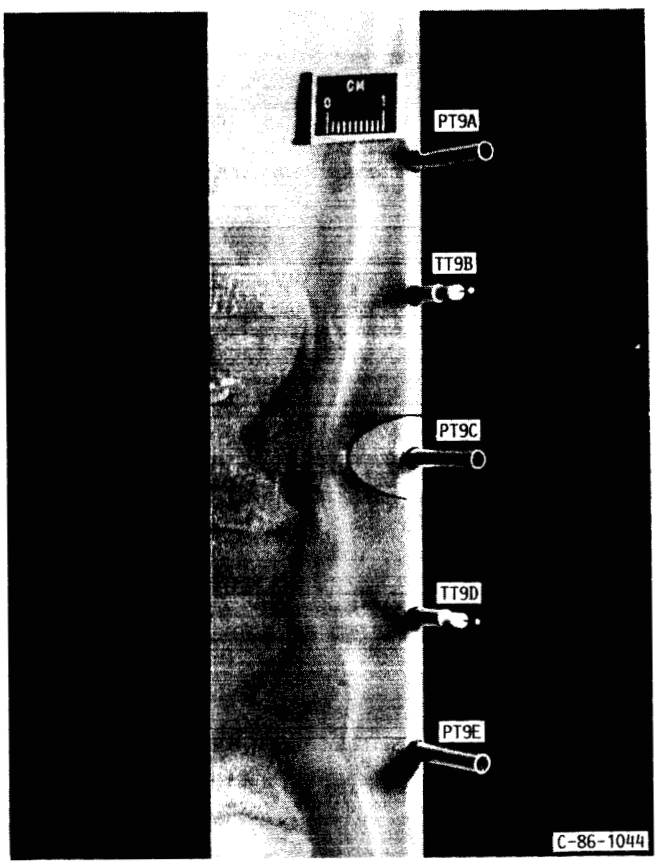

FIGURE 3. - TRAVERSING PROBE INSTRUMENTATION CONFIGURATION.

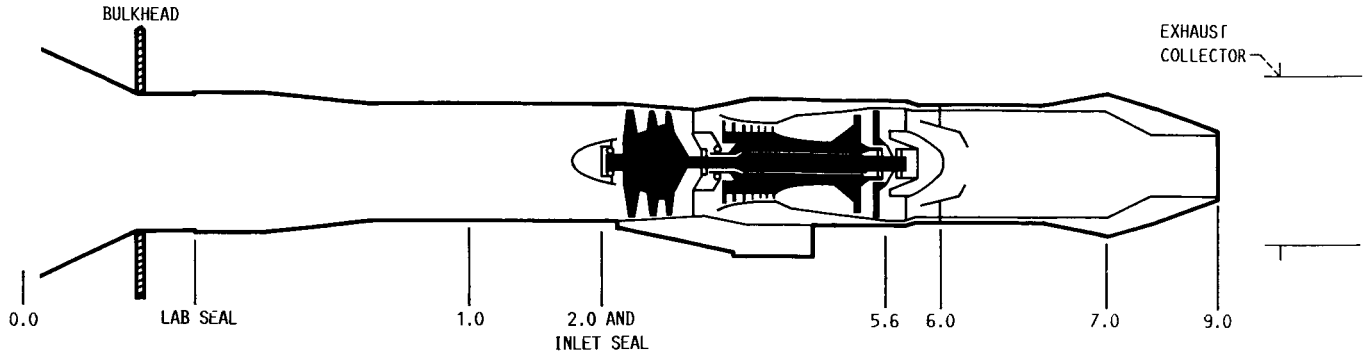

STATION NUMBER	DESCRIPTION
0.0	INLET PLENUM
1.0	AIRFLOW STATION
2.0	ENGINE INLET
5.6	TURBINE EXIT
6.0, 7.0	A/B LINER
9.0	EXIT OF NOZZLE

(A) STATION LOCATIONS.

FIGURE 4. - SCHEMATIC OF ENGINE INSTALLATION AND INSTRUMENTATION STATIONS.

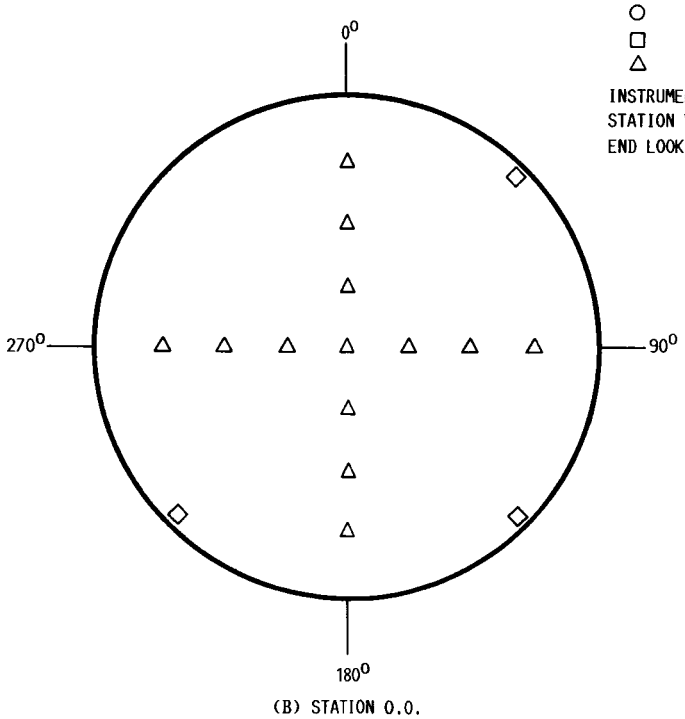

(B) STATION 0.0.

○ TOTAL PRESSURE
□ STATIC PRESSURE
△ TEMPERATURE

INSTRUMENTATION AT EACH STATION VIEWED FROM AFT END LOOKING FORWARD

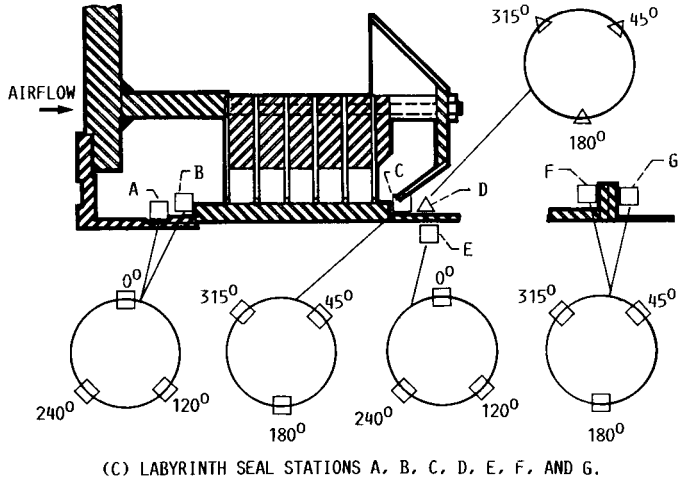

(C) LABYRINTH SEAL STATIONS A, B, C, D, E, F, AND G.

FIGURE 4. - CONTINUED.

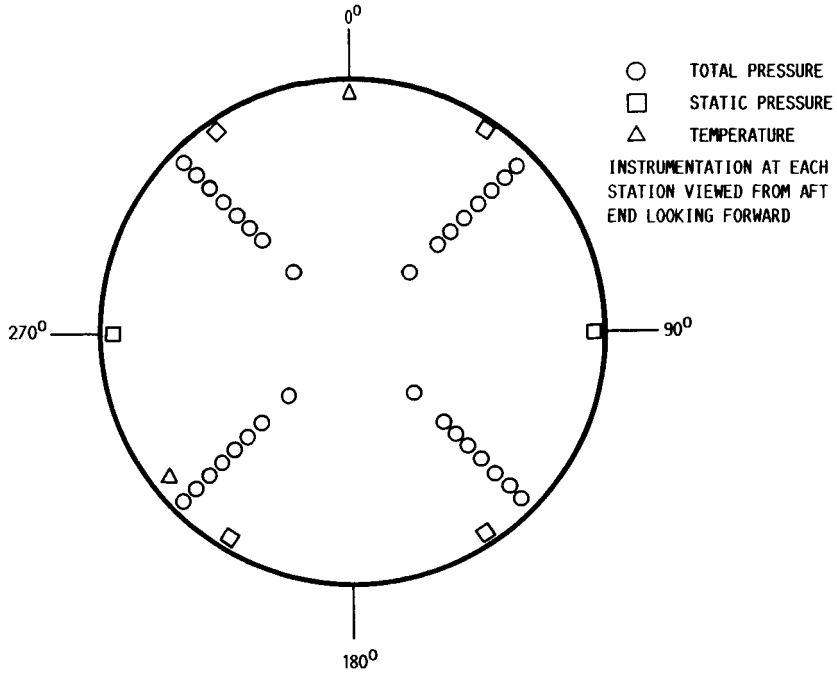

(D) STATION 1.0.

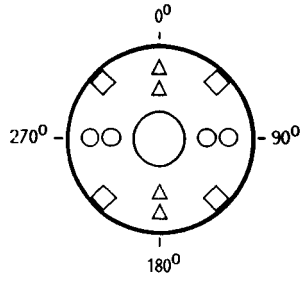

(E) STATION 2.0.

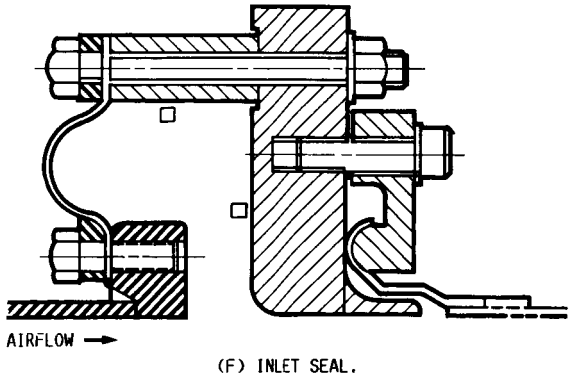

(F) INLET SEAL.

FIGURE 4. - CONTINUED.

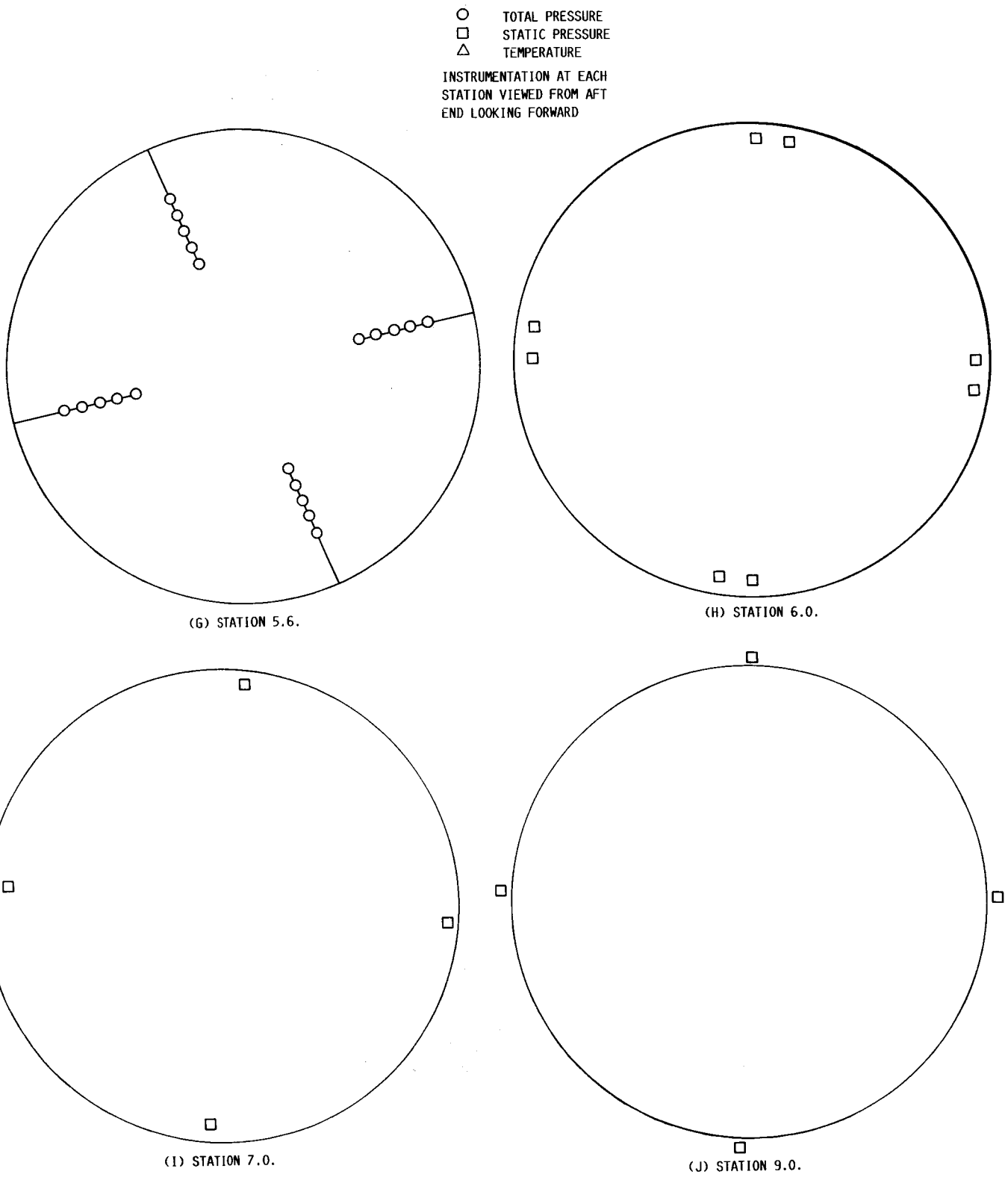

FIGURE 4. - CONCLUDED.

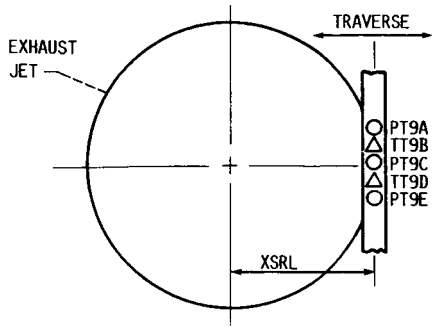

(A) RAKE TRAVERSE ACROSS EXHAUST JET HORIZONTAL RADIUS.

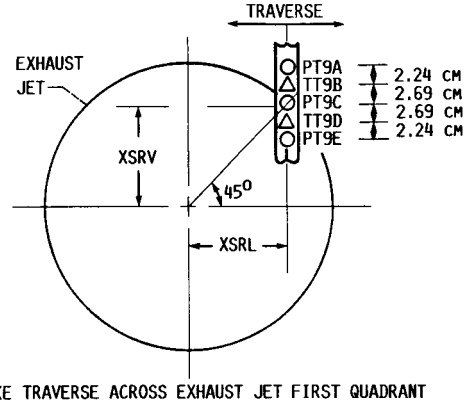

(B) RAKE TRAVERSE ACROSS EXHAUST JET FIRST QUADRANT (LOOKING UPSTREAM).

FIGURE 5. - EXHAUST GAS JET SURVEY.

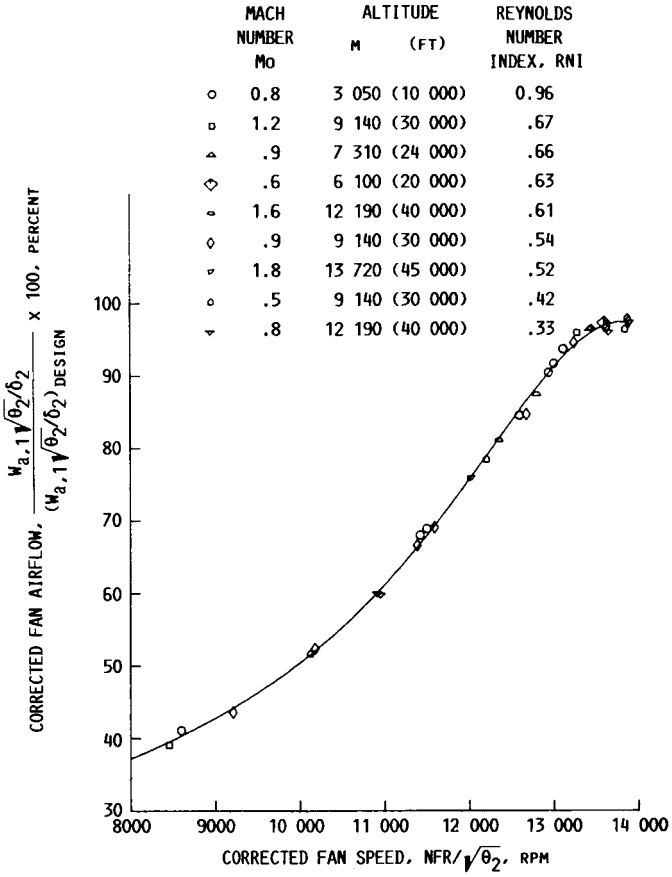

FIGURE 6. - CORRECTED AIRFLOW AS A FUNCTION OF CORRECTED FAN SPEED, STANDARD DAY.

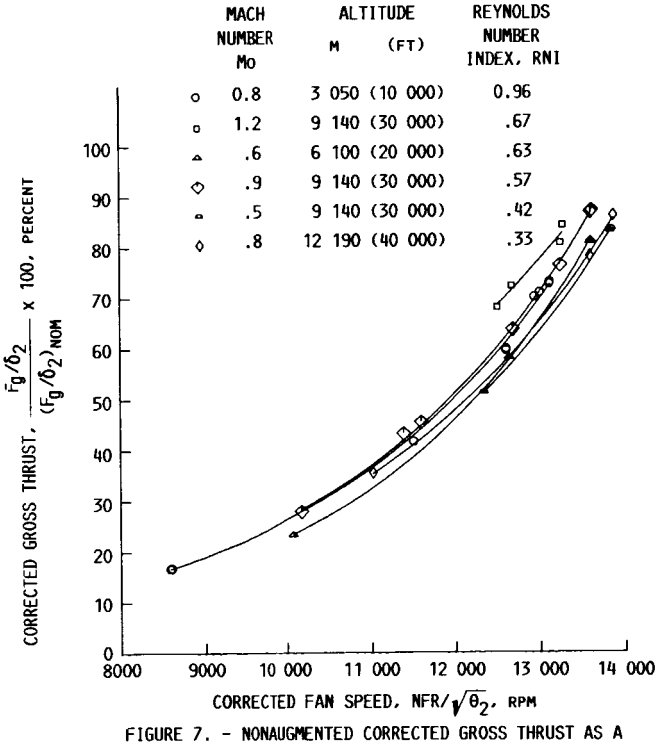

FIGURE 7. - NONAUGMENTED CORRECTED GROSS THRUST AS A FUNCTION OF CORRECTED FAN SPEED, STANDARD DAY.

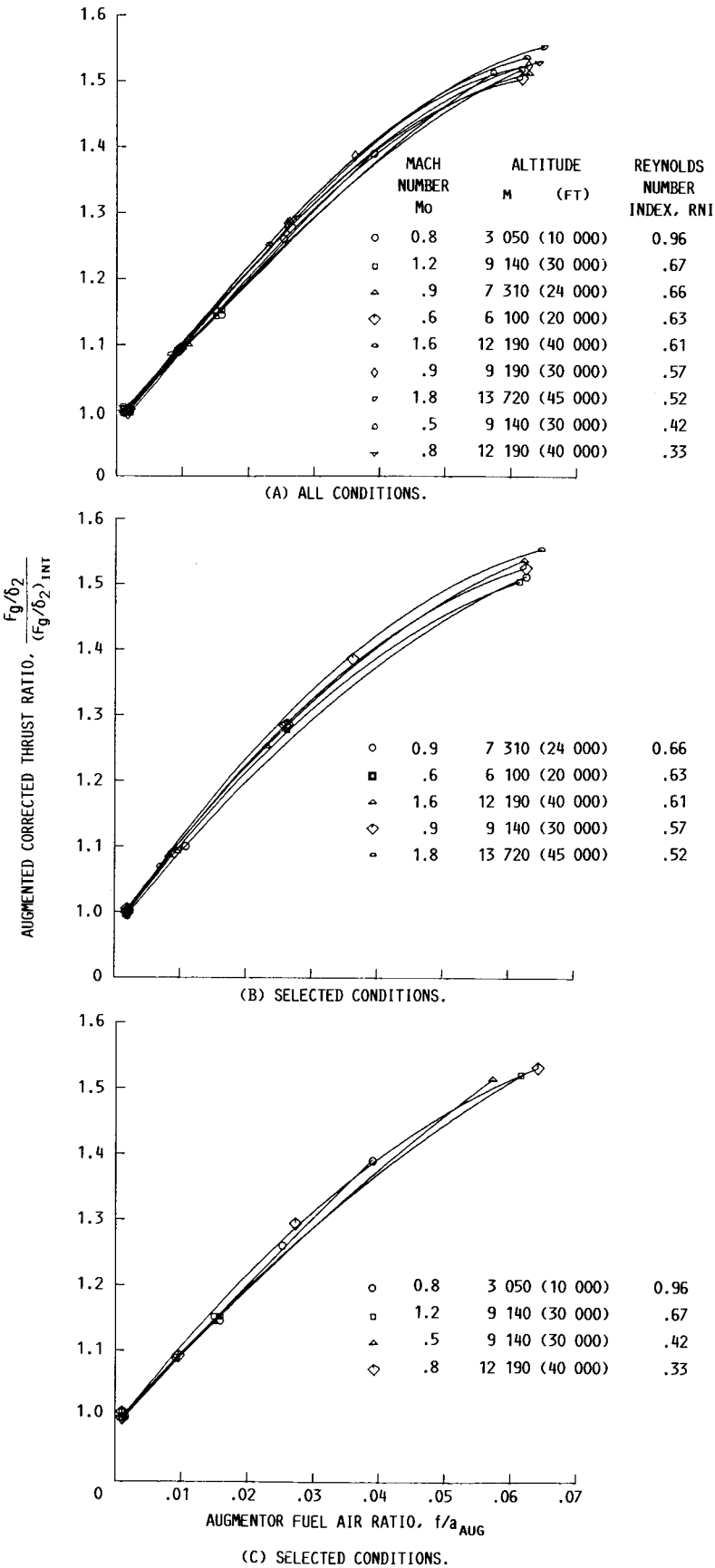

FIGURE 8. - AUGMENTED THRUST AS A FUNCTION OF FUEL AIR RATIO, STANDARD DAY.

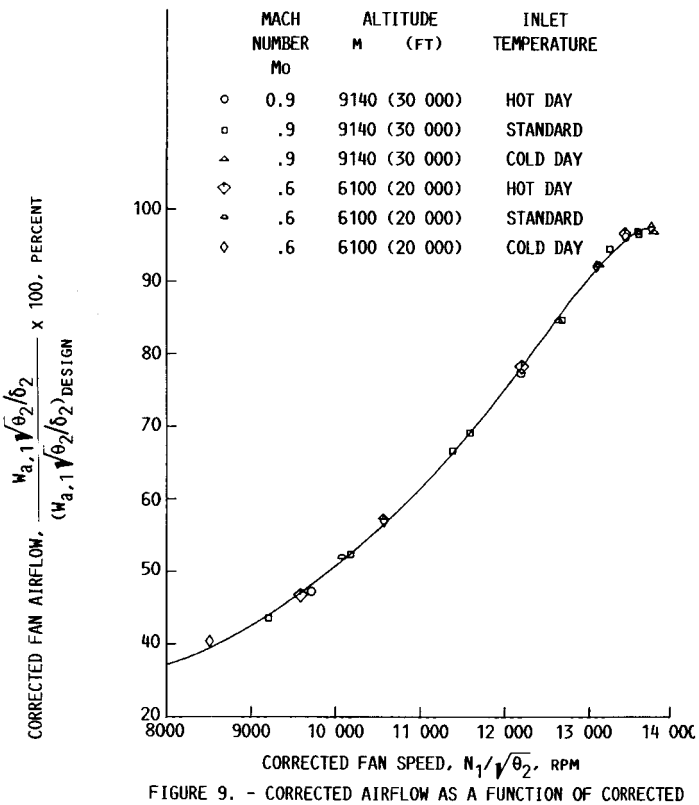

FIGURE 9. - CORRECTED AIRFLOW AS A FUNCTION OF CORRECTED FAN SPEED OVER A RANGE OF INLET TEMPERATURES, NON-STANDARD DAY.

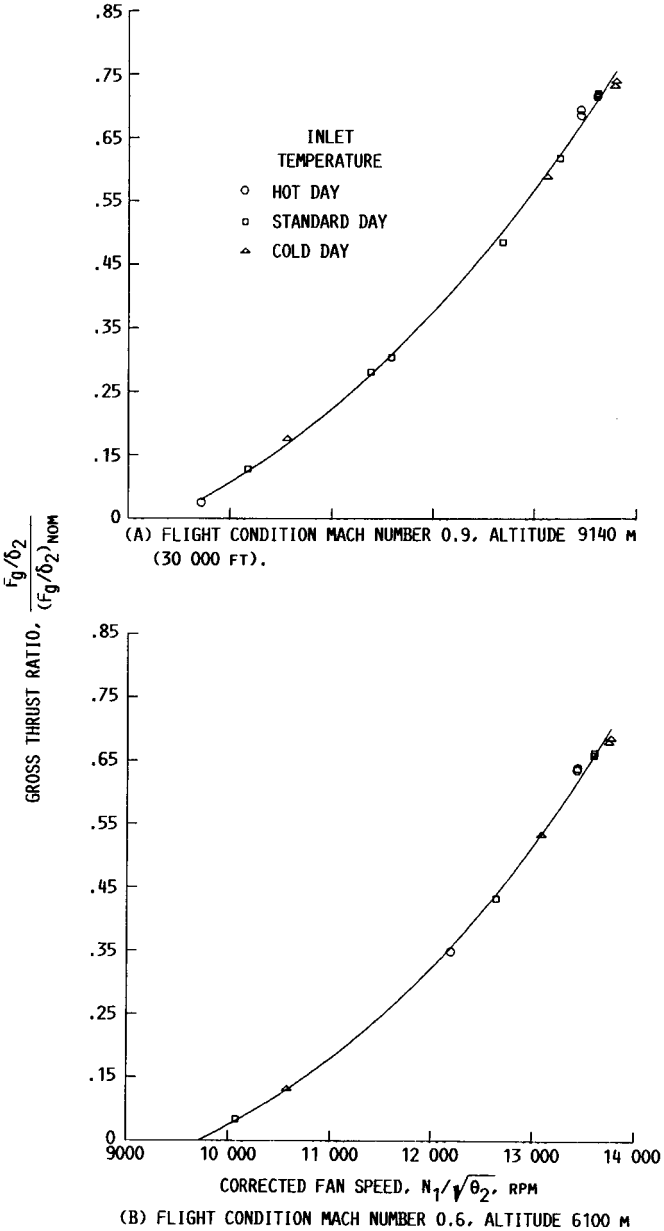

(A) FLIGHT CONDITION MACH NUMBER 0.9, ALTITUDE 9140 M (30 000 FT).

(B) FLIGHT CONDITION MACH NUMBER 0.6, ALTITUDE 6100 M (20 000 FT).

FIGURE 10. - CORRECTED NONAUGMENTED GROSS THRUST AS A FUNCTION OF CORRECTED FAN SPEED, OVER A RANGE OF INLET TEMPERATURES.

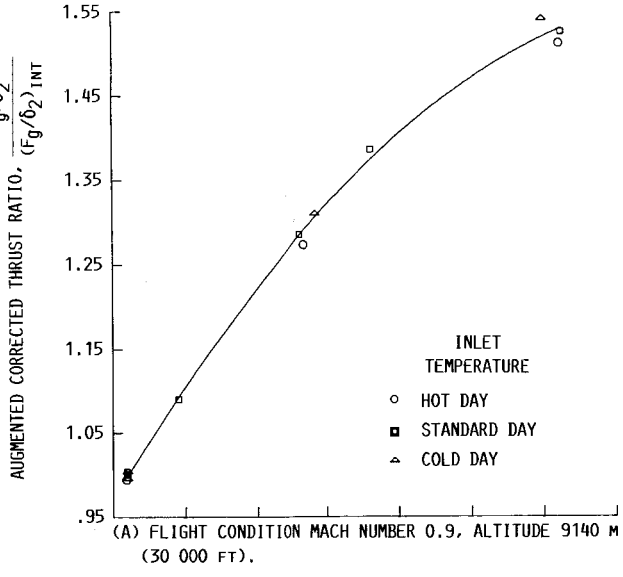

(A) FLIGHT CONDITION MACH NUMBER 0.9, ALTITUDE 9140 M (30 000 FT).

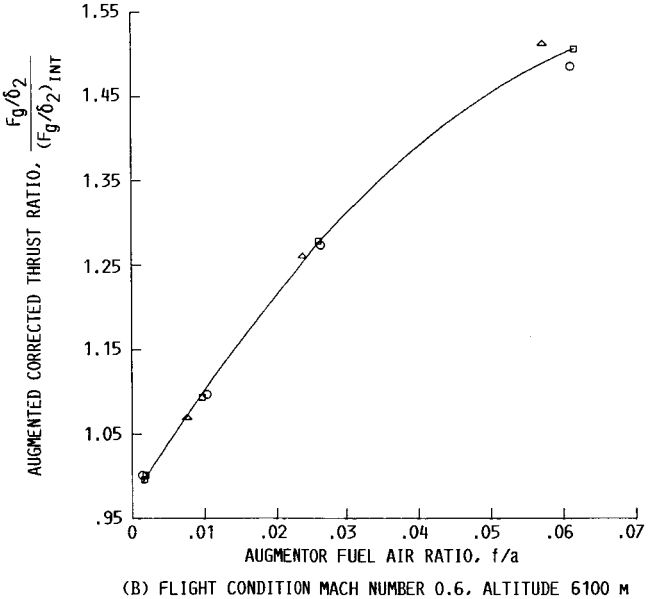

(B) FLIGHT CONDITION MACH NUMBER 0.6, ALTITUDE 6100 M (20 000 FT).

FIGURE 11. - AUGMENTED THRUST RATIO AS A FUNCTION OF FUEL AIR RATIO OVER A RANGE OF INLET TEMPERATURES.

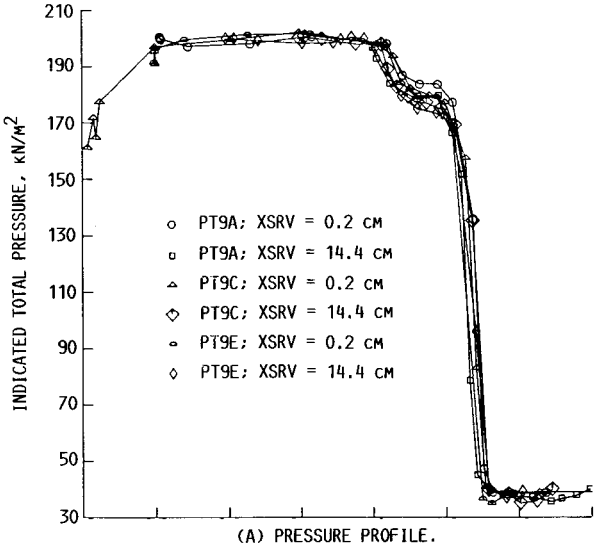

(A) PRESSURE PROFILE.

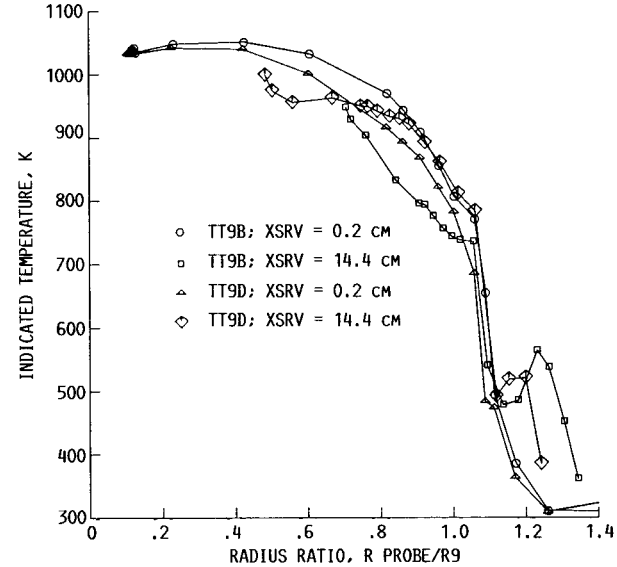

(B) TEMPERATURE PROFILE.

FIGURE 12. - EXHAUST GAS SURVEY AT TEST CONDITION 5. MILITARY POWER SETTING; CALCULATED R9 = 24.20 CM.

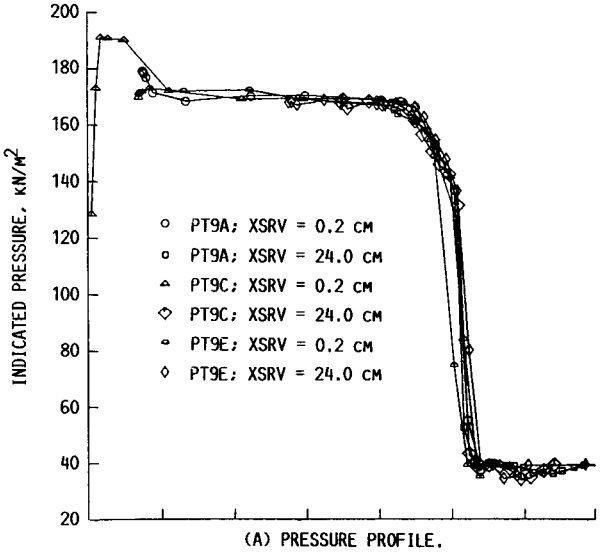

(A) PRESSURE PROFILE.

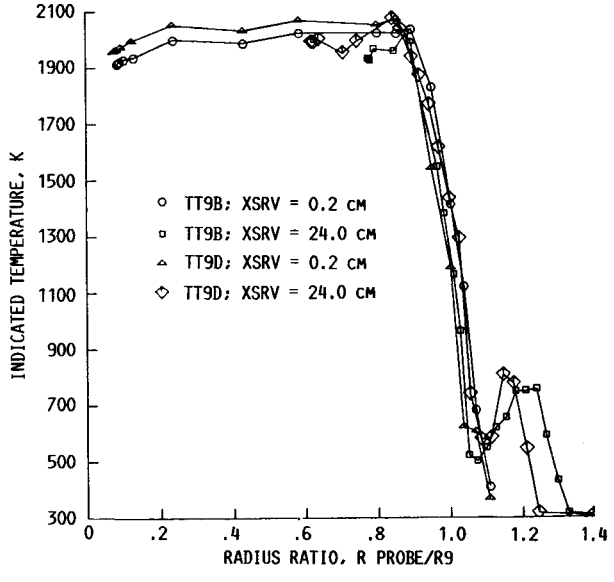

(B) TEMPERATURE PROFILE.

FIGURE 13. - EXHAUST GAS SURVEY AT TEST CONDITION 5. MAXIMUM AFTERBURNING POWER SETTING; CALCULATED R9 = 34.42 cm.

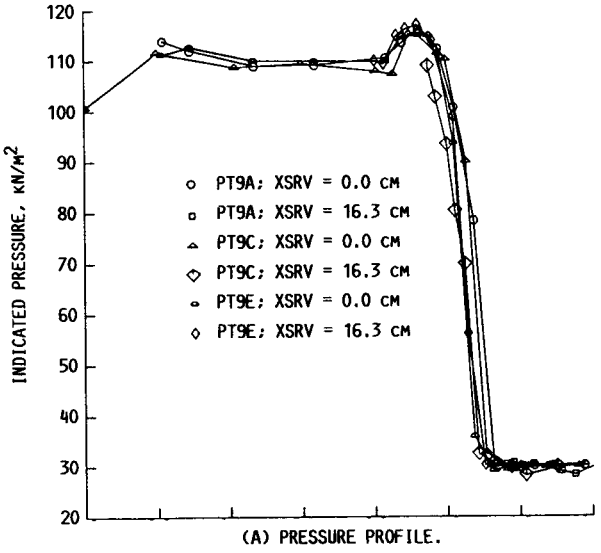

(A) PRESSURE PROFILE.

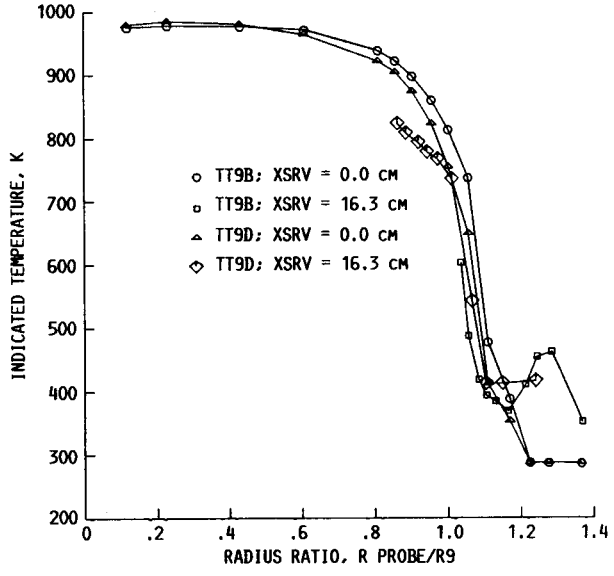

(B) TEMPERATURE PROFILE.

FIGURE 14. - EXHAUST GAS SURVEY AT TEST CONDITION 6. MILITARY POWER SETTING; CALCULATED R9 = 23.04 cm.

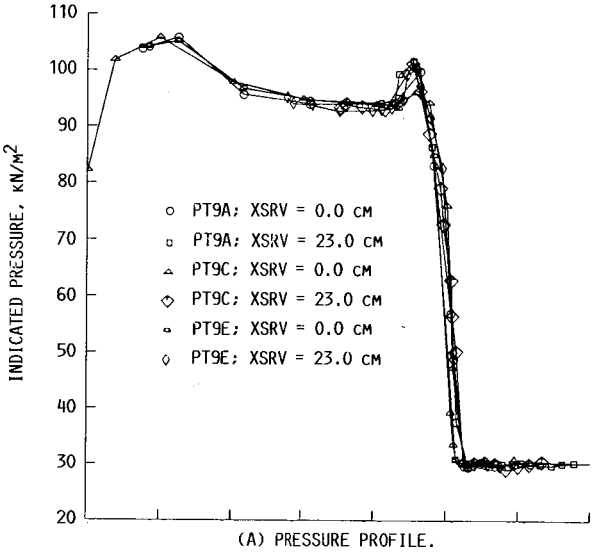

(A) PRESSURE PROFILE.

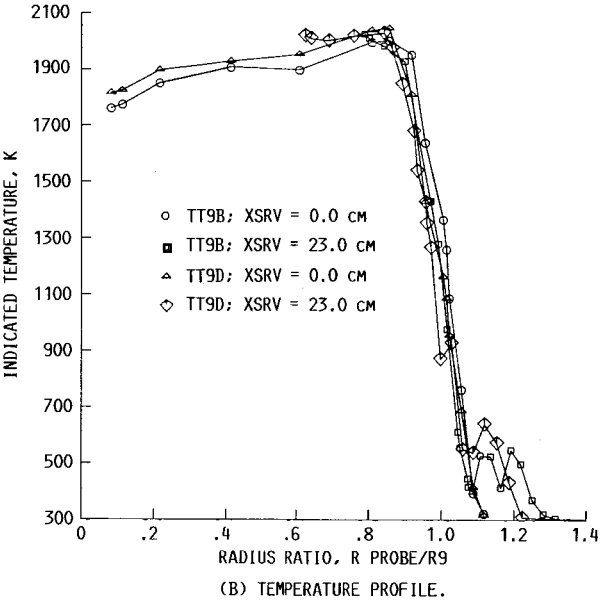

(B) TEMPERATURE PROFILE.

FIGURE 15. - EXHAUST GAS SURVEY AT TEST CONDITION 6. MAXIMUM AFTERBURNING POWER SETTING: CALCULATED R9 = 32.71 cm.

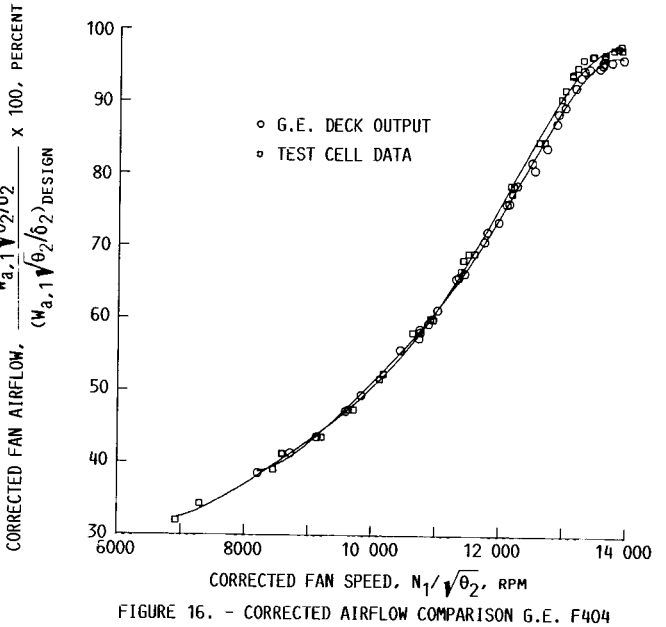

FIGURE 16. - CORRECTED AIRFLOW COMPARISON G.E. F404 SPEC DECK VERSUS TEST CELL DATA.

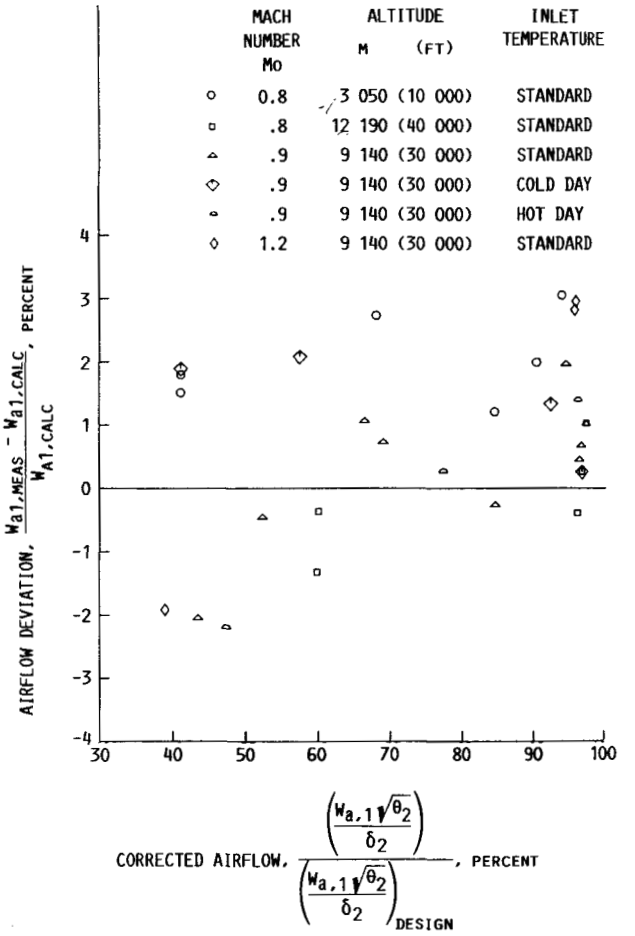

FIGURE 17. - CORRECTED AIRFLOW DEVIATION.

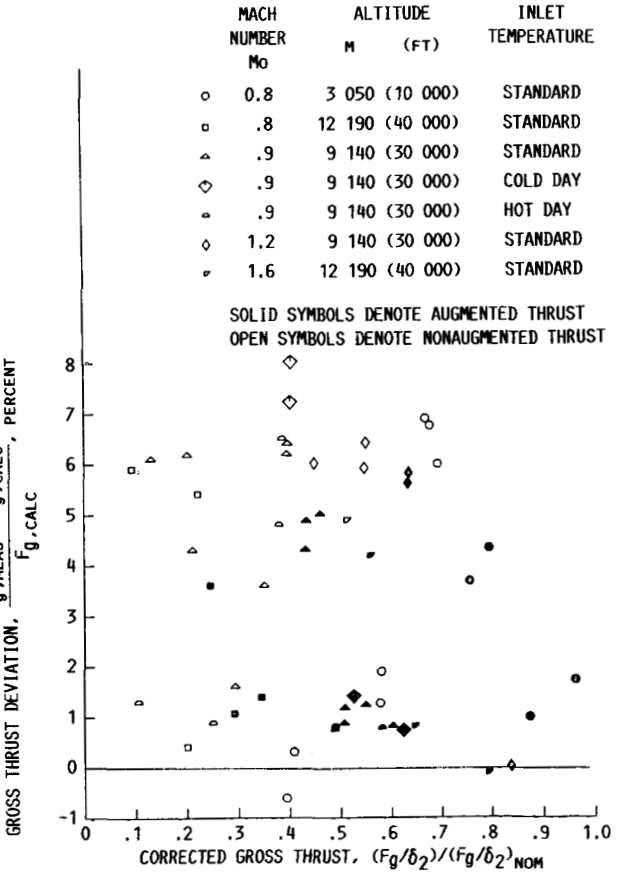

FIGURE 18. - CORRECTED THRUST DEVIATION.

NASA
National Aeronautics and Space Administration

Report Documentation Page

1. Report No.	2. Government Accession No.	3. Recipient's Catalog No.
NASA TM-100159		

4. Title and Subtitle
Airflow Calibration and Exhaust Pressure/Temperature Survey of an F404, S/N 215-109, Turbofan Engine

5. Report Date
September 1987

6. Performing Organization Code
505-62-3B

7. Author(s)
Maureen E. Burns and Thomas A. Kirchgessner

8. Performing Organization Report No.
E-3447

10. Work Unit No.

9. Performing Organization Name and Address
National Aeronautics and Space Administration
Lewis Research Center
Cleveland, Ohio 44135

11. Contract or Grant No.

13. Type of Report and Period Covered
Technical Memorandum

12. Sponsoring Agency Name and Address
National Aeronautics and Space Administration
Washington, D.C. 20546

14. Sponsoring Agency Code

15. Supplementary Notes

16. Abstract

A General Electric F-404 turbofan engine was calibrated for thrust and airflow at the NASA Lewis Propulsion System Laboratory in support of future flight tests of the X-29 aircraft. Tests were conducted with and without augmentation, over a range of flight conditions, including the two design points of the airplane. Data obtained during the altitude tests will be used to correct two independent gross thrust calculation routines which will be installed and operated on the airplane to determine in-flight gross thrust. Corrected airflow data as a function of corrected fan speed collapsed onto a single curve. Similarly, trends were observed and defined for both augmented and dry thrust. Overall agreement between measured data and F-404 Engine Spec Deck data was within 2 percent for airflow and 6 percent for thrust. The results of an uncertainty analysis for thrust and airflow is presented. In addition to the thrust calibration, the exhaust gas boundary layer pressure and temperatures were surveyed at selected condition and engine power levels to obtain data for another NASA F-404 program. Test data for these surveys are presented.

17. Key Words (Suggested by Author(s))	18. Distribution Statement
F-404; X-29; Thrust; Airflow calibration; Altitude test facility; Exhaust gas survey	Unclassified - unlimited STAR Category 07

19. Security Classif. (of this report)	20. Security Classif. (of this page)	21. No of pages	22. Price*
Unclassified	Unclassified	30	A03

NASA FORM 1626 OCT 86

*For sale by the National Technical Information Service, Springfield, Virginia 22161